Nanosecond laser therapy reverses pathologic and molecular changes in age-related macular degeneration without retinal damage

A. I. Jobling,*[,1] R. H. Guymer,[†,1] K. A. Vessey,* U. Greferath,* S. A. Mills,* K. H. Brassington,[†] C. D. Luu,[†] K. Z. Aung,[†] L. Trogrlic,* M. Plunkett,[‡] and E. L. Fletcher*[,2]

*Department of Anatomy and Neuroscience, The University of Melbourne, Victoria, Australia; [†]Centre for Eye Research Australia, University of Melbourne, Royal Victorian Eye and Ear Hospital, Victoria, Australia; and [‡]Ellex R&D Pty Ltd, Adelaide, Australia

ABSTRACT **Age-related macular degeneration (AMD) is a leading cause of vision loss, characterized by drusen deposits and thickened Bruch's membrane (BM). This study details the capacity of nanosecond laser treatment to reduce drusen and thin BM while maintaining retinal structure. Fifty patients with AMD had a single nanosecond laser treatment session and after 2 yr, change in drusen area was compared with an untreated cohort of patients. The retinal effect of the laser was determined in human and mouse eyes using immunohistochemistry and compared with untreated eyes. In a mouse with thickened BM (ApoEnull), the effect of laser treatment was quantified using electron microscopy and quantitative PCR. In patients with AMD, nanosecond laser treatment reduced drusen load at 2 yr. Retinal structure was not compromised in human and mouse retina after laser treatment, with only a discrete retinal pigment epithelium (RPE) injury, and limited mononuclear cell response observed. BM was thinned in the ApoEnull mouse 3 mo after treatment (ApoEnull treated 683 ± 38 nm, ApoEnull untreated 890 ± 60 nm, C57Bl6J 606 ± 43 nm), with the expression of *matrix metalloproteinase-2* and *-3* increased (>260%). Nanosecond laser resolved drusen independent of retinal damage and improved BM structure, suggesting this treatment has the potential to reduce AMD progression.—Jobling, A. I., Guymer, R. H., Vessey, K. A., Greferath, U., Mills, S. A., Brassington, K. H., Luu, C. D., Aung, K. Z., Trogrlic, L., Plunkett, M., Fletcher, E. L. Nanosecond laser therapy reverses pathologic and molecular changes in age-related macular degeneration without retinal damage. *FASEB J.* 29, 696–710 (2015). www.fasebj.org**

Key Words: vision loss · drusen · Bruch's membrane · matrix metalloproteinase

AGE-ASSOCIATED DISEASE is an increasing health concern worldwide, with the global population over 60 expected to more than double over the next 40 yr (1). Visual impairment is a major component of age-associated disease, particularly AMD, which is the leading cause of irreversible vision loss in Europe, the United States, and Australia and responsible for approximately 50% of legal blindness in these countries (2, 3). AMD is principally a disease of the central retina, or macula; however, its cellular pathology is varied, affecting the light-sensitive photoreceptors within the retina; their supporting cells; the RPE; BM, which separates the blood supply (choroid) from the RPE/photoreceptor complex; and the choroidal blood supply itself (4, 5). With time, the disease progresses to 1 of 2 late forms; geographic atrophy ("dry" or atrophic AMD), which is characterized by areas of photoreceptor and RPE degeneration, and neovascular ("wet") AMD, which generally occurs when choroidal vessels penetrate BM, invade the outer retina, and hemorrhage resulting in a dramatic loss of vision (4). Although the recent use of VEGF inhibitors have proven successful at arresting the progression of wet AMD (6–8), there is no treatment currently available for those with geographic atrophy and little to offer as an intervention to slow progression of the earlier stages of disease.

Early stages of AMD are typically asymptomatic with respect to vision, and progression to the later vision-threatening forms of the disease is usually slow, providing ample opportunity to intervene. Although several studies have identified serum (9) and urine (10) biomarkers of early disease, the presence of drusen remains a classic marker of the early stages of AMD, signifying risk of vision loss from the later forms of the disease (11, 12). These extracellular deposits are observed between the RPE and BM and present as yellowish deposits under fundoscopy (13–15). Studies have shown that the type, size, and extent of drusen are predictors of AMD progression (16–18). A

Abbreviations: AMD, age-related macular degeneration; BM, Bruch's membrane; RPE, retinal pigment epithelium; OCT, optical coherence tomography; SD-OCT, spectral domain optical coherence tomography; FAF, fundus autofluorescence; PNA, peanut agglutinin; C3, complement factor 3; Mmp, matrix metalloproteinase; Hprt, hypoxanthine guanine phophoribosyl transferase; Gapdh, glyceraldehyde-3-phosphate dehydrogenase; ONL, outer nuclear layer; OPL, outer plexiform layer; IPL, inner plexiform layer

[1] These authors contributed equally to this work and should be considered joint first authors.

[2] Correspondence: Department of Anatomy and Neuroscience, The University of Melbourne, Grattan St., Parkville 3010, Victoria, Australia. E-mail: elf@unimelb.edu.au.

doi: 10.1096/fj.14-262444

This article includes supplemental data. Please visit *http://www.fasebj.org* to obtain this information.

0892-6638/15/0029-0696 © FASEB

second hallmark sign of AMD, although not detectible *via* clinical tools, is a thickened BM, which is accompanied by an accumulation of lipid-rich deposits and reduced transport across the membrane (19–21). These early markers of AMD have led to the hypothesis that BM thickening and drusen accumulation reflect a disruption of nutrient and waste transfer between the photoreceptors/RPE complex and the choroidal vasculature, leading to the photoreceptor degeneration (22). Thus, treatments that resolve drusen and thin BM may prove helpful in limiting progression of AMD.

Although regulation of BM function has been reported *in vitro* (23) and chronic administration of statins has recently been shown to inhibit BM thickening in a high fat atherogenic mouse model (24), there is currently no clinically appropriate treatment for reversing BM change in AMD. By contrast, the reabsorption of drusen following treatment by ophthalmic lasers has been well documented (14, 25–27). However, the exact mechanism used to resolve drusen is unclear, with endothelial cell interaction (28), the presence of phagocytic cells (29), and release of soluble factors from the RPE (30, 31) all implicated. Despite the ability of some lasers to reduce drusen, the effect on AMD progression is equivocal, with some studies showing an improvement (32, 33) and others reporting no effect (27, 34); some even suggest an acceleration of disease (35). The lack of any definitive effect on AMD progression may have resulted from the additional inherent retinal injury caused by these thermal lasers (36).

Recently, a low-energy, subthreshold, nanosecond laser has been designed to induce a targeted RPE injury, which is independent of retinal neuronal damage or significant retinal gliosis (37–39). This laser has been tested in patients with diabetic macular edema with promising results (40). Our group has recently reported on the use of this nanosecond laser in a group of patients with intermediate AMD and reported that a single unilateral application of the laser results in improved macular appearance and function (41). What is not clear from these studies is the mechanism by which nanosecond laser treatment induces change, and whether this provides a rationale for exploring the use of this laser treatment for reducing progression of AMD.

The aim of this study was to characterize the mechanism by which nanosecond laser treatment affects the retina. Specifically, a pilot clinical trial was undertaken to determine the efficacy of nanosecond laser treatment in reducing drusen load, and the structural effect of the laser was characterized in human and mouse retina. Using an animal model that recapitulates the thickened BM seen in AMD, the effect of nanosecond laser treatment on BM thickness and RPE-choroidal gene expression was also characterized.

MATERIALS AND METHODS

Human studies

A nonrandomized prospective pilot clinical study was established (Australian New Zealand Clinical Trials Registry, ID: ACTRN12609001056280) to determine the effect of nanosecond laser treatment in the early stages of AMD. The 12 mo data for fundus appearance and macula function has recently been published (41). Fifty participants (50–75 yr) with bilateral intermediate AMD (drusen $>$ 125 μm) (11) and best corrected visual acuity of 20/63, were enrolled in the trial after written informed consent was obtained. After baseline examination, incorporating slit-lamp microscopic assessment, fundus examination, photography (Canon CR-DGi; Canon Incorporated, Tokyo, Japan), and spectral domain optical coherence tomography (SD-OCT; Cirrus; Carl Zeiss Meditec, Jena, Germany), the worst-performing eye was treated with a nanosecond, ultra-low-energy laser (3ns, 2RT laser; Ellex, Adelaide, SA, Australia). Each patient received, in a single session, 12 laser spots (400 μm spot diameter) placed around the macula ($>$500 μm from the fovea), with energy levels individually titrated to be below the visual threshold for retinal change (range 0.15–0.45 mJ, average energy 0.24 mJ). In the current study, a natural history cohort was included for comparison of drusen resolution and consisted of 58 untreated subjects with AMD who had the same inclusion criteria as the treated group. All individuals were reviewed at 6 mo intervals for 2 yr.

In addition to the clinical trial, the effect of the nanosecond laser on the human retina/RPE was characterized in an 83-yr-old individual whose right eye was removed as part of an exenteration operation for an aggressive lid malignancy. Five days prior to exenteration, a full baseline examination was performed and multimodal retinal imaging performed. Six laser spots (400 μm diameter) were delivered to the superior macula just below the superior arcade at an energy of 0.3 mJ, which was considered the clinically relevant dose. An additional 6 suprathreshold spots (defined as 2$\times$ clinical dose, 0.6 mJ) were delivered to the inferior macula just above the inferior arcade. A second human eye was taken from an 84-yr-old individual who had been diagnosed with a lid basal cell carcinoma. Treatment was as described previously; however, nanosecond laser was performed at 2 time points, 1 mo and 1 wk prior to exenteration. Fundus photographs and OCT images were taken before and immediately after treatment as well as just prior to the surgery. For human studies, ethical approval was obtained from the Human Ethics Committee of the Royal Victorian Eye and Ear Hospital and studies were conducted in adherence with the Declaration of Helsinki.

Animal experiments

The effect of the nanosecond laser on mouse retinal structure was investigated using 3-mo-old C57BL/6J (general retinal structure) and Cx3cr1$^{GFP/+}$ (on a C57BL/6J background; mononuclear cell response) animals. Cx3cr1$^{GFP/+}$ animals have 1 copy of the microglial/macrophage-specific gene, *Cx3cr1*, replaced by the gene for enhanced green fluorescent protein (*EGFP*) (42). These heterozygote animals are functionally normal, yet allow the morphology of microglial cells to be easily assessed.

All animals were anesthetized (ketamine: xylazine, 67:13 mg/kg), received additional corneal anesthesia (0.5%; Alcaine; Alcon Laboratories, Hünenberg, Switzerland), and were bilaterally dilated (1% atropine sulfate; Alcon Laboratories). The nanosecond laser was used to deliver 20 spots (each 0.065 mJ) around the optic nerve in 1 eye, with the untreated fellow eye serving as a "within animal" control. Laser energy was determined in a similar manner to that used for human clinical application (the dose below the visual threshold for a retinal response = pseudoclinical dose). A second cohort of animals received a 20 suprathreshold (0.13 mJ; 2$\times$ the pseudoclinical dose) spots, and untreated age-matched untreated control animals (C57BL/6J, Cx3cr1$^{GFP/+}$) were also included. The retinal fundus was imaged (Micron III; Phoenix Research Labs, Pleasanton, CA, USA) before and after laser treatment. Animals were allowed to recover, and tissue was isolated at 1, 5, and 24 h and 7 d post-treatment.

The ApoEnull model of AMD was used to assess the efficacy of the nanosecond laser on reducing BM thickness, a key pathologic change observed in patients with AMD. ApoEnull animals have

the apolipoprotein gene, *ApoE,* inactivated by gene-specific targeting (43) and were obtained from the Animal Resources Centre (Murdoch, WA, Australia). Animals were aged for 10 mo ($n = 18$) after which time a subset was anesthetized as above and unilaterally treated with 20 laser spots ($n = 9$, 0.065 mJ) and allowed to recover. A group of age-matched C57BL/6J animals was similarly treated. Tissue was isolated 3 mo post-laser treatment. All animals were housed at < 40 lux, with access to food and water *ad libitum.* Animal experiments were approved by the University of Melbourne Animal Ethics Committee and adhered to the American Association of Vision Research and Ophthalmology standards for the ethical treatment of animals.

Quantification of drusen resolution

Drusen area was determined by 2 masked graders, using gold standard methods of estimating drusen area based upon color fundus photographs (44). Images centered on the fovea (3000 μm radius) were taken at baseline, 12 mo, and 24 mo, and the macular was divided into 5 concentric circles, with each circle divided into 4 quadrants. The percentage of drusen area was calculated within each of these regions with drusen area compared at different time points and classed as the same (drusen area ± 5% of baseline), better (decrease in drusen area >5%), or worse (increase in drusen area > 5%) than baseline area. These results were subsequently reviewed by an independent grader, masked to the first results. The drusen regression data for the 12 mo time point has been previously published (41); however, the addition of the natural history cohort allows the efficacy of the laser treatment to be determined. This was not previously possible. The proportions of laser-treated and untreated fellow eyes with reduced drusen area were compared with that observed in the natural history. Any eyes that had progressed to late disease (geographic atrophy, choroidal neovascularization) were excluded from further analysis of drusen area (see **Table 1**) (41).

Assessment of RPE change within areas of drusen regression

A subset of patients with AMD who had shown drusen regression after nanosecond laser treatment (n = 12) had fundus autofluorescence (FAF) images assessed at baseline, 12 mo, and 24 mo (Spectralis HRA+OCT; Heidelberg Engineering, Heidelberg, Germany). FAF imaging principally measures the autofluorescence of bisretinoid compounds in the RPE, provides information on the physiologic state of the RPE/outer retina, and is a marker for AMD progression to geographic atrophy (45, 46). Images were analyzed using the method of Toy *et al.* (47). Briefly, baseline, color fundus images were registered and the 12 and 24 mo images subtracted from baseline (ImageJ, 1.43 Freeware; National Institutes of Health, Bethesda, MD, USA) (48). Specific areas of drusen regression were identified, and these areas were superimposed onto the FAF images. The distribution of grayscale levels was calculated within the identified area and compared with background measures (Supplemental Fig. 1). A pixel was determined to have increased autofluorescence when it exceeded the mean background grayscale level by 3 SD. Similarly, when the level was 3 SD less than the mean background level, its intensity was decreased (Supplemental Fig. 1). The extent of autofluorescence was then determined for baseline, 12 mo, and 24 mo images and classified as increased, decreased, or no change (levels equal ± 5%).

TABLE 1. *The effect of nanosecond laser treatment on the development of advanced AMD-related disease*

Time post-treatment (mo)	Natural history eyes	Nanosecond laser-treated eyes	Fellow untreated eyes
12	6/116 (5%)	3/50 (6%)	2/50 (4%)
24	10/116 (9%)	4/50 (8%)	3/50 (6%)

The efficacy of nanosecond laser treatment was assessed in a pilot clinical study involving 50 individuals with intermediate AMD (drusen > 125 μm) and compared with a natural history cohort (58 individuals) with the same inclusion criteria. All underwent baseline visual assessment and were free of signs of advanced AMD (geographic atrophy/choroidal neovascularization). Data showing the progression to advanced forms of AMD are presented, with relevant percentages shown in parentheses. Of those that had progressed to late stage disease, all in the treated group showed evidence of geographic atrophy, and the natural history cohort exhibited geographic atrophy or choroidal neovascularization (3/3 at 12 mo, 7/3 at 24 mo).

Tissue processing, immunohistochemistry, histology

Following laser treatment, human eyes were exenterated (5 d and 1 mo post-treatment), the anterior section removed at the limbus, and the posterior eyecup immediately placed in 4% paraformaldehyde (in 0.1 M phosphate buffer, pH 7.4) for 5 h. Following fixation, the eyecup was placed in phosphate buffer, carefully dissected into multiple regions and cryoprotected (graded sucrose in 0.1 M phosphate buffer, 10%, 20%, 30%). Mouse eyes (C57BL/6J, Cx3cr1$^{GFP/+}$) were enucleated, and the posterior eyecup was isolated as above. Tissues were placed in 4% paraformaldehyde for 30 min, washed in 0.1 M phosphate buffer, and cryoprotected as above. Samples were embedded in Tissue-Tek (Microm International GmbH, Walldorf, Germany) optimum cutting temperature frozen and vertically sectioned (14 μm) onto polysine slides (Menzel-Glaser, Braunschweig, Germany).

Sections were processed for fluorescent immunohistochemistry as previously described (49, 50). To investigate the effect of the nanosecond laser on retinal structure, human sections were coincubated with a rhodamine-conjugated peanut agglutinin (PNA; 1:250; Vector Laboratories, Burlingame, CA, USA) to label cone photoreceptors and an antibody to calbindin (mouse anti-calbindin, 1:2000; Swant, Marly, Switzerland), which labels multiple cell types in the human retina (51). Sections were subsequently incubated with a goat anti-mouse Alexa Fluor 488 secondary antibody (1:500; Molecular Probes, Incorporated, Eugene, OR, USA). To assess mononuclear cell response, human sections were labeled with the mononuclear marker, ionized calcium-binding adapter molecule 1 (rabbit anti-IbA1, 1:1500; Wako Pure Chemical Industries, Richmond, VA, USA) and subsequently reacted with a goat anti-rabbit secondary antibody conjugated to Alexa Fluor 488 (1:500; Molecular Probes). Cx3cr1$^{GFP/+}$sections were labeled with Alexa Fluor 488–conjugated anti-GFP (goat; Rockland Immunochemicals, Gilbertsville, PA, USA). Complement factor 3 (C3) expression was determined using a rat monoclonal anti-C3 antibody (1:100; Abcam, Cambridge, United Kingdom) and a goat anti-mouse Alexa Fluor 594 (1:500; Molecular Probes). To determine cell death in the mouse retina following nanosecond laser treatment, TUNEL was performed as per manufacturers' instructions (Roche Diagnostics, Basel, Switzerland). All cell nuclei were counterstained with DAPI (0.2 μg/ml; Life Technologies, Carlsbad, CA, USA).

Human and mouse tissues were also processed in whole mount, with the fixed retinae gently dissected away from the respective tissue sections/eyecups. For RPE structural analysis (human, C57BL/6J), RPE tissue samples were incubated overnight at 4°C with a conjugated antibody to the filamentous actin label, phalloidin (Alexa Fluor 633 Phaloidin, 1:200; Life Technologies), and whole-mount Cx3cr1$^{GFP/+}$ retinae were incubated

with Alexa Fluor 488-conjugated anti-GFP (Rockland Immunochemicals). All retinal sections and retinal/RPE whole mounts were mounted (Dako, Glostrup, Denmark), imaged using a confocal microscope (Meta or Pascal LSM-5, Zen software; Zeiss, Jena, Germany).

Microglial morphology was quantified at 1, 5, and 24 h and 7 d post-laser treatment, with Z-stack images isolated from the outer plexiform layer (OPL; 10 images per retina, $n = 5$ retinae) around the optic nerve (<1750 μm diameter), which included the laser-treated areas. Cell morphology was assessed using Metamorph software (Molecular Devices, Sunnyvale, CA, USA), and microglial process extension into the outer segment was quantified after 24 h ($n = 4$, ImageJ) and 3-dimensional renderings produced *via* Imaris image software (Biplane, Zurich, Switzerland). RPE cell size and wound diameter were quantified at 1, 5, 24 h and 7 d, and the number of TUNEL-positive cells were quantified 24 h after laser treatment ($n = 3$, per retinal area, ImageJ).

For retinal histology, posterior eyecups from C57BL/6J animals were fixed overnight (1% paraformaldehyde, 2.5% glutaraldehyde, 3% sucrose, 0.01% calcium chloride in 0.1 M phosphate buffer, pH 7.4), washed in 0.1 M phosphate buffer, and then dehydrated in methanol (75, 85, 95, and 100%) and acetone (100%). Tissues were embedded (Epon resin; ProSciTech, Townsville City, QLD, Australia), polymerized, and sectioned (1 μm, Ultracut S; Reichert, Depew, NY, USA). Retinal sections were stained with 1% toluidine blue and imaged (Axioplan; Zeiss, Göttingen, Germany) (52).

Electron microscopy

Transmission scanning electron microscopy was used to investigate RPE/BM structure in C57BL/6J and ApoEnull animals following nanosecond laser treatment. Posterior eye cups were isolated as above and fixed overnight (1% paraformaldehyde, 2.5% glutaraldehyde, 3% sucrose, 0.01% calcium chloride in 0.1 M phosphate buffer, pH 7.4). They were subsequently washed in 0.1 M cacodylate buffer pH 7.4, incubated for 1 h in 1% OsO_4 in cacodylate buffer, dehydrated, and embedded (Epon resin). Ultrathin sections (70 nm) were cut and collected on formvar-coated copper grids. Sections were contrasted with uranyl acetate and lead citrate solutions, and viewed with a Phillips CM120 electron microscope (FEI, Hillsboro, OR, USA) (49). For analysis of BM thickness, 5–7 micrographs were taken for each ApoEnull and C57BL/6J animal in the control, laser treated, and untreated fellow eye cohorts (each $n = 6$ per group). Membrane thickness measurements were taken at 5 separate locations within each image and subsequently averaged (at least 25 measures per animal).

RNA isolation and quantitative PCR

For gene expression analysis, posterior eyecups from C57BL/6J and ApoEnull animals were isolated as described for immunohistochemical analysis. Retinae were removed from the posterior eyecup and snap frozen in liquid nitrogen. RPE-choroidal samples were isolated after the addition of 50 μl lysis buffer (RLTplus, RNeasy mini; Qiagen, Valencia, CA, USA) containing 2-mercaptoethanol (1%), snap frozen in liquid nitrogen, and stored at −80°C.

Total RNA was isolated from the RPE-choroidal samples using commercial spin columns (RNeasy, Qiagen). A PCR gene array was used to assess the expression of 84 genes involved extracellular matrix (ECM) regulation (ECM and adhesion molecule array; Qiagen). Briefly, ApoE total RNA samples from untreated, laser-treated eyes and untreated fellow eyes ($n = 9$ each group, each 25 ng) were pooled within their respective treatment groups (3 independent experiments containing 3 pooled samples), reverse transcribed (RT^2 first strand; Qiagen) and then underwent preamplification of the cDNA target templates (RT^2 pre-AMP; Qiagen). Samples were added to a commercial master mix (RT^2 SYBR green master mix; Qiagen) and amplified for 40 cycles (ABI 7900HT; Life Technologies, Grand Island NY, USA). Three independent arrays were performed for each treatment group. The data were analyzed using $\Delta\Delta$Ct, expressed as fold change and regulation assessed using an unpaired *t* test.

Matrix metalloproteinase-2 and *-3* (*Mmp-2* and *Mmp-3*) gene expression was quantified in all treatment groups using quantitative PCR ($n = 9$ each group). Total RNA samples from RPE/choroid (40 ng) were reverse transcribed (Sensiscript; Qiagen) and amplified (Rotor-Gene SYBR Green PCR kit; Qiagen) using specific primers (*Mmp2*: forward 5′-gtcgcccctaaaacagacaa-3′, reverse 5′-ggtctcgatggtgttctggt-3′; *Mmp3*: forward 5′-cagacttgtcccgtttccat-3′, reverse 5′-ggtgctgactgcatcaaaga-3′). External standards were used for quantification of gene copy number as previously described (50), using the housekeeping genes, hypoxanthine guanine phophoribosyl transferase (*Hprt;* forward 5′-cctaagatgagcgcaagttgaa-3′, reverse 5′-ccacaggactagaacacctgctaa-3′), and glyceraldehyde-3-phosphate dehydrogenase (*Gapdh; f*orward 5′-tgtgtccgtcgtggatctga-3′, reverse 5′-ttgctgttgaagtcgcaggag-3′). Data were expressed as copies/copy *Hprt*.

Statistical analysis

In the pilot clinical trial, the proportion of laser-treated and untreated fellow eyes with reduced drusen area was compared with that observed in the natural history group using χ^2 test. All quantitative data from immunohistochemical and histologic studies were compared with untreated controls and assessed using *t* tests and 1- or 2-way ANOVAs where appropriate (see figure legends for specific test). Quantitative data from electron micrographs and real-time quantitative PCR were compared using a 2-way ANOVA and further assessed with a Bonferroni *post hoc* test.

RESULTS

Drusen resolution in patients with AMD following nanosecond laser treatment

Sub-RPE drusen deposits are classic markers of AMD and are also used in the assessment of disease progression (12, 16). To determine the capacity of the nanosecond laser to reduce drusen in those with AMD, 50 individuals with intermediate AMD (drusen >125 μm) underwent baseline visual assessment and had 12 nanosecond laser spots (Ellex 2RT laser) delivered unilaterally to the macula. Multimodal *in vivo* imaging was used to grade drusen change up to 2 y post-treatment. **Figure 1** shows the fundus of one participant pre-laser treatment (Fig. 1*A*) with distinct yellow drusen present in and around the macula. Using SD-OCT, these sub-RPE deposits can be observed in retinal cross section (see arrows in Fig. 1*C*), and the disruptive nature of drusen on the RPE monolayer is evident in the RPE contour (Fig. 1*E*) and heat (Fig. 1*G*, red = greater displacement) maps. When the same retinal area was reassessed 12 mo after nanosecond laser treatment, the fundus image showed a reduction in drusen number and area in and around the macula (B), and this regression was supported by the SD-OCT scan (Fig. 1*D*) and subsequent multimodal analysis (Fig. 1*F, H*).

Although several individuals showed complete resolution of drusen deposits similar to that shown in Fig. 1*A–H*, not all participants exhibited such complete resolution

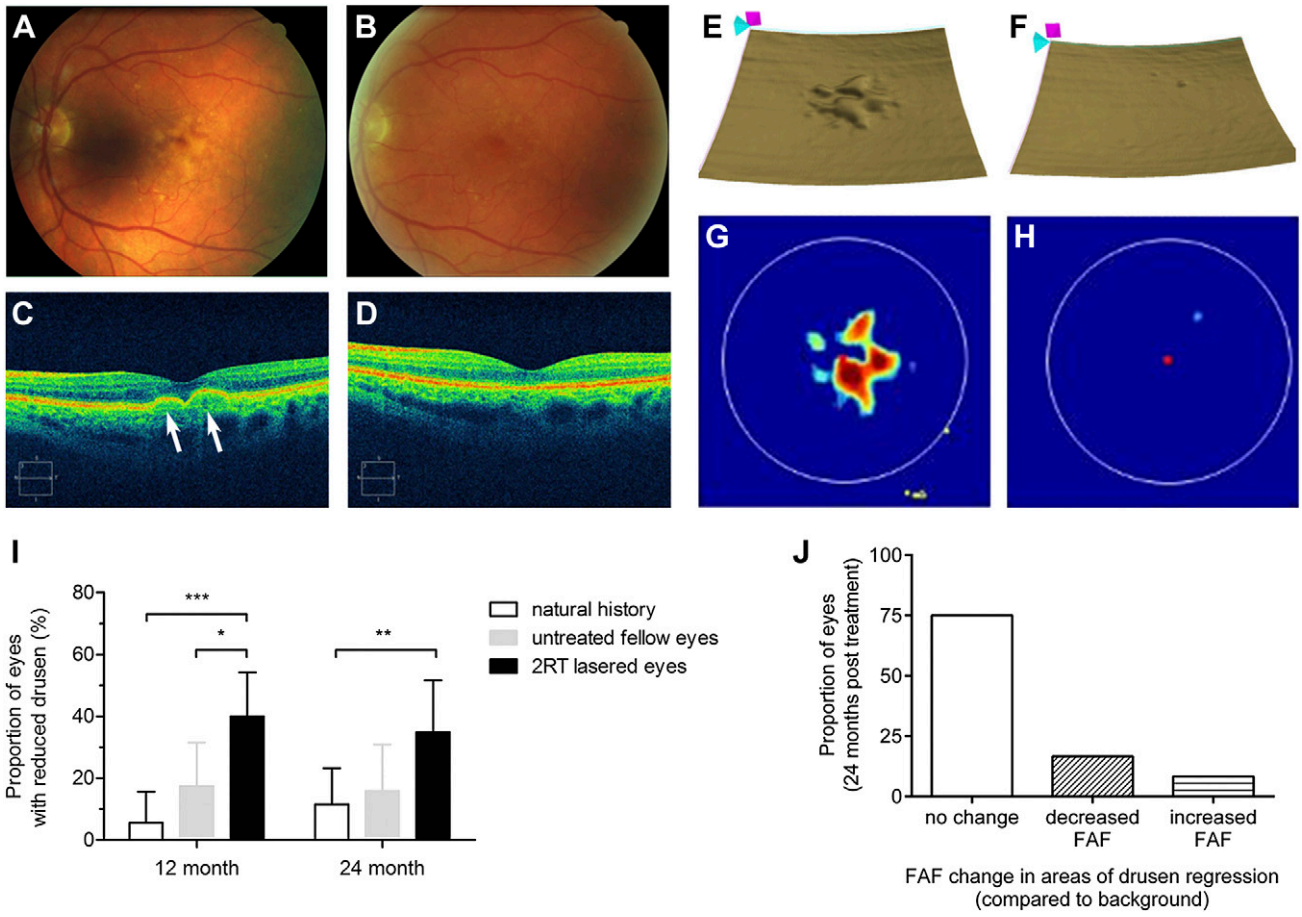

Figure 1. Drusen resolution following nanosecond laser treatment. Multimodal image analysis was performed on a 74-yr-old woman with intermediate AMD using a Cirrus SD-OCT. Images were taken of the left eye before (*A, C, E, G*) and 12 mo after (*B, D, F, H*) nanosecond laser treatment. Color fundus photographs were taken (*A, B*) and the extent of drusen (pale yellow deposits in central retina, *A*) imaged using OCT (*C, D*), a segmented RPE map (*E, F*) and a drusen elevation heat map (*G, H*). At 12 mo following laser treatment, there was a substantial reduction in the extent of drusen in this participant. When the full cohort was analyzed for the proportion of individuals showing a reduction in drusen area (*I*), there was a significant reduction at 12 and 24 mo compared with a nature history cohort. When FAF images were assessed in regions of drusen resolution and compared with background areas within the same macula, most individuals (75%) showed stable FAF images, and the remaining individuals showed either increased or decreased autofluorescence, indicative of RPE/photoreceptor dysfunction and or loss (*J*). For autofluorescence data (*J*), $n = 12$. The 12 mo treated and fellow eye drusen resolution data have been previously published (41).Error bars represent the upper 95% confidence interval; $n > 43$ individuals analyzed using a χ^2 test. *$P = 0.05$, **$P < 0.01$, ***$P < 0.001$.

(see Supplemental Fig. 2, also see Guymer *et al.*) (41). To assess the cohort effect, drusen regression was quantified in the treated and untreated fellow eyes in the nanosecond laser-treated cohort and compared with an age-matched natural history cohort. After 12 mo, of those who had not reached a form of late disease (see Table 1), 40% of treated eyes had a reduction in drusen area in the treated eye compared with baseline measurements. Although these 12 mo data have been previously reported (41), the inclusion of the natural history cohort allows the efficacy of the treatment to be statistically validated. When compared, the percentage of eyes that showed a reduction at 12 mo was significantly greater than the 5% reduction observed in the natural history cohort ($P < 0.001$). This positive effect was maintained at the 24 mo time point, with 35% of the treated eyes showing regression, and only 11% of eyes in the natural history cohort exhibited less drusen ($P < 0.01$). Interestingly, the untreated fellow eye in the nanosecond laser-treated group also showed a regression in drusen compared with the natural history cohort at 12 mo ($P = 0.05$); however, this effect was not significant at 24 mo ($P > 0.05$). Fellow eye alterations after monocular laser treatment have been previously reported after treatment for AMD and glaucoma (44, 53).

Spontaneous drusen regression in AMD has been linked in some patients with disease progression, involving RPE atrophy and outer retinal change (47, 54). To determine whether the RPE showed pathologic alterations in areas of drusen regression, FAF imaging was analyzed in a subset of laser-treated eyes 24 mo after treatment and compared with baseline images. Data indicated that 75% of eyes showed no alteration in autofluorescence in areas where drusen had resolved, and the remaining 25% of eyes showed either a decrease (16.7%) or increase (8.3%) in FAF readings compared with baseline after drusen regression (Fig. 1*J*). As decreased FAF is indicative of RPE cell loss (geographic atrophy) and increased FAF reflects lipofuscin accumulation (precedes RPE damage), any change in the autofluorescence profile would be suggestive of AMD progression (55). Thus, the nanosecond

laser-induced reduction in drusen load appeared independent of the RPE change in the majority of patients, implying no indication of AMD progression to atrophy.

Preservation of retinal structure following nanosecond laser treatment

Traditional thermal ophthalmic lasers, although resolving drusen, also lead to neuronal injury and death in the overlying retina. In some cases, these treatments alter BM integrity, hastening disease progression (25, 35). This collateral damage may reduce the effectiveness of lasers to limit AMD progression. Previous reports in the rat and pig retina suggest that this nanosecond laser produces little retinal damage (37–39); however, its effect on the human retina is unknown. To address this, nanosecond laser treatment was performed on the right eye of an 83-yr-old individual 5 days prior to a scheduled exenteration procedure for the presence of an aggressive eyelid malignancy. Six laser spots were delivered to the macula just below the superior vascular arcade at 0.3 mJ (a clinically relevant dose), and 6 suprathreshold spots (0.6 mJ) were delivered to the macula, just above the inferior vascular arcade. The fundus photograph taken after treatment (**Fig. 2*A***) shows a macula, with the suprathreshold spots evident as discrete bleached areas of retina (arrowheads and box D). The superior, clinically relevant laser doses are less clear upon fundus examination (box C).

Immediately after exenteration (5 d post-laser treatment) the enucleated eye was fixed and vertical sections taken through the 0.3 mJ (box C in fundus, shown in Fig. 2*C*) and suprathreshold (box D in fundus, shown in Fig. 2*D*) laser-treated areas. Retinal structure was assessed using the cone photoreceptor marker PNA (red) and calbindin (green), which labels multiple neuronal cell types in the human retina (51). When compared with an untreated area of the retina (Fig. 2*B*), the area of the retina directly over the 0.3 and 0.6 mJ laser spots was unaffected, with no major structural change nor neuronal death evident (Fig. 2*C, D*, respectively). Of particular interest, the outer segments of the cone photoreceptors (outer region of the outer nuclear layer [ONL]) remain unaltered by the laser treatment, despite being situated directly over the laser-treated RPE (also see Supplemental Fig. 3*E*). Yet although the outer segments show no indication of degeneration, accumulated cells can be seen in close contact with the tips of the outer segments within the treated region (see arrows in Fig. 2*C, D*).

Mouse models are particularly useful when investigating the mechanism or treatment of ocular diseases (56). To determine whether mouse retina was equally resistant to the nanosecond laser and provide a basis for the use of this laser on a mouse model of AMD, adult C57BL/6J mice were treated with a 0.065 mJ laser dose to approximate the clinical condition in the human eye. It should be noted that although the same clinical criteria for determining laser energy dose was used in mouse experiments, the differences in dose (*i.e.,* 0.065 mJ *vs.* 0.3 mJ) reflect the differences in pigmentation, eye size, and optics of a mouse eye compared with that of a human. As can be observed from the fundus photo (Fig. 2*E*), the 0.065mJ dose produced a larger and more obvious bleached area within the mouse retina compared with the human, with this effect likely due to the greater degree of RPE pigmentation found in the C57BL/6J mouse eye. Despite this degree of bleaching, the retinal structure over the treated area remained unaffected when compared with an untreated retinal section (Fig. 2*F vs. G*). To determine whether nanosecond laser treatment could result in retinal damage, a higher laser dose was used (0.13 mJ). After this high-dose treatment, the mouse retina exhibited significant disruption, particularly in the ONL, with most of the cells in that layer lost (Fig. 2*H*). Retinal cell death (TUNEL, red) was assessed after the 0.065 mJ (Fig. 2*I*) and 0.13 mJ (Fig. 2*J*) treatments, with most of the cell death found in the high-energy treatment confined to the ONL (see Fig. 2*J*). When cell death was quantified (Fig. 2*K*), the 0.065 mJ laser dose produced no significant retinal cell death compared with the untreated control (100 ± 52 *vs.* 41 ± 30 cells /mm^2, $P > 0.05$), while numerous TUNEL-positive cells were present in the 0.13 mJ treatment (4064 ± 907 cells/mm^2 retina, $P < 0.01$). Thus, like in the human eye, low-energy nanosecond laser treatment does not lead to retinal damage in the mouse; however, when laser energies are significantly increased, retinal cell death can occur.

Nanosecond laser treatment targets the RPE

Previous work on porcine and rat retina suggests the nanosecond laser specifically targets the RPE monolayer underneath the retina (37, 38); however, there is no information regarding the tissue specificity in the human. Flat-mounted retinal sections from the laser-treated human eye were stained with the filamentous actin label phalloidin (red) and the RPE monolayer was imaged (**Fig. 3*A–C***). The normal human RPE monolayer has a highly ordered polygonal appearance (Fig. 3*A*), and areas of RPE treated with the clinically relevant laser dose (0.3 mJ) showed a disrupted monolayer (Fig. 3*B*). When treated with suprathreshold laser dose (0.6 mJ), more distinct RPE lesions or holes are evident within the monolayer (Fig. 3*C*). Similar RPE lesions were present in the mouse eye, with the highly ordered RPE monolayer (Fig. 3*D*) disrupted by low-dose nanosecond laser treatment (0.065 mJ; Fig. 3*E*), and a more defined injury occurred in the high-energy group (0.13 mJ; Fig. 3*F*).

To investigate the RPE wound healing response, a human eye was obtained that had previously been treated with nanosecond laser on 2 separate occasions (1 mo and 1 wk) prior to exenteration. Imaging the RPE monolayer with phalloidin (red) at the region treated with nanosecond laser 1 wk prior to collection showed the presence of enlarged RPE cells on the lesion boundary, with some cells extending into the injury site (Fig. 3*G*). At 1 mo post-treatment, the lesion site was completely covered with enlarged RPE cells (Fig. 3*H*).

A similar process was evident within the mouse eye, although healing was more rapid, with a significant reduction in lesion area evident within 24 h, and the RPE monolayer was intact within 1 wk (0.065 mJ; Fig. 3*J*, 3*I*). At 7 d, cells covering the injury site were 289% larger (1112 ± 99 *vs.* 385 ± 26 μm^2, $P < 0.01$) than RPE cells from untreated retinae (Fig. 3*I, K*). As well as increasing in size, some of the RPE cells surrounding the laser injury site were also positive for the cell proliferation marker cyclinD1 (Fig. 3*L*), while the surrounding untreated RPE showed no evidence of cyclinD1 staining.

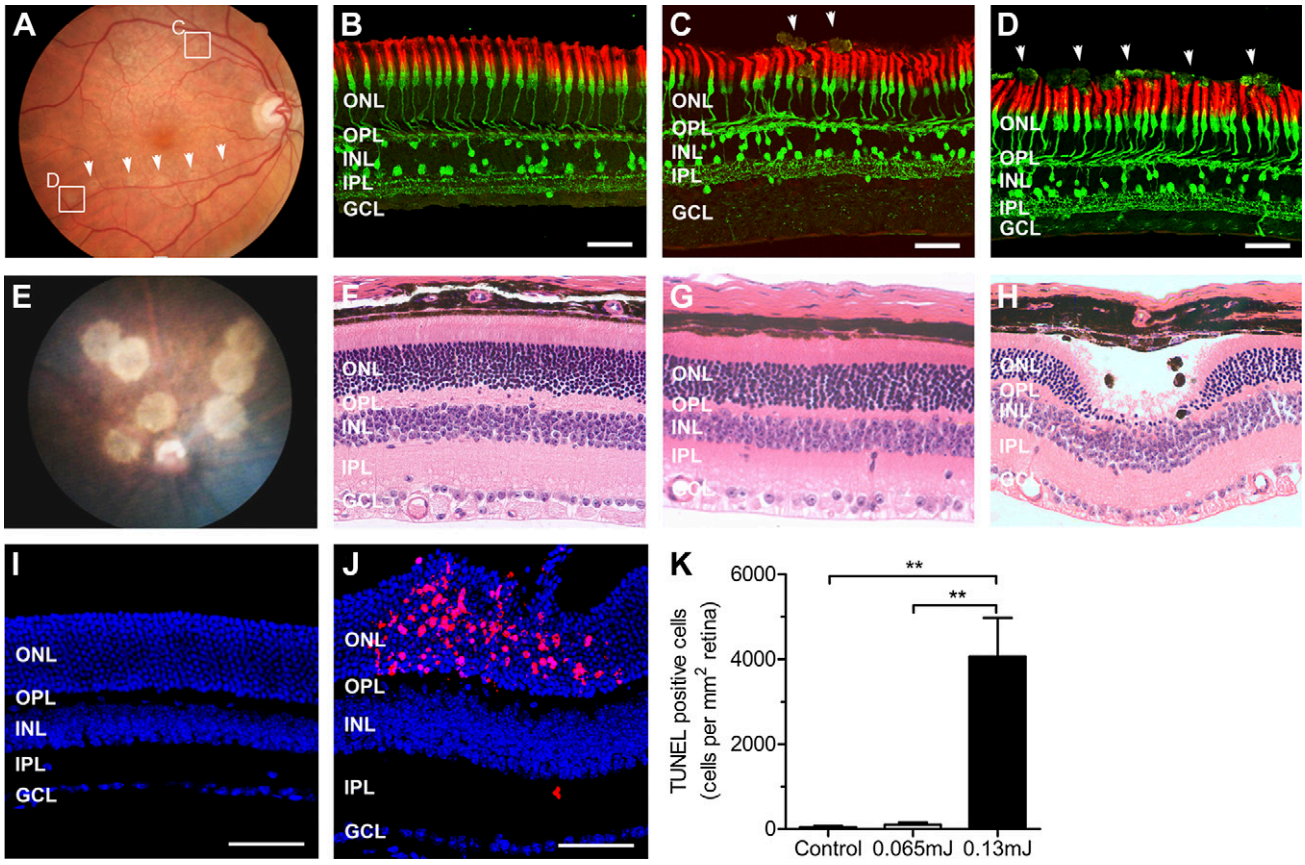

Figure 2. Human and mouse retinal structure following nanosecond laser treatment. An 83-yr-old patient had 6 clinically relevant (0.3 mJ) and 6 suprathreshold (0.6 mJ) (arrows) nanosecond laser spots delivered to the superior and inferior macula respectively (*A*, fundus photo). After 5 d, the eye was surgically removed, immediately fixed and areas of retina corresponding to the clinical (C box) and suprathreshold (D box) doses were sectioned. Retinal structure was assessed using the cone photoreceptor marker, PNA (red) and calbindin (green), which labels numerous cell types in the human retina. Neither the clinical (*C*) nor suprathreshold (*D*) treatments altered retinal structure when compared with retinal areas disparate from the laser treatment sites (*B*); however, cells were observed in close association with the photoreceptor outer segments at the laser site (arrows). Mouse eyes were treated with 0.065 mJ and 0.13 mJ laser doses (*E*, fundus photo) and although the lower dose (*G*) produced no alteration in retinal structure compared with untreated retina (*F*), the higher dose led to significant disruption in the outer retina (*H*). Retinal cell death was assessed using TUNEL (red) 24 h following laser treatment in the low- (*I*) and high-energy (*J*) cohorts, and sections were counterstained with the nuclear label, DAPI (blue). The extent of TUNEL was quantified showing the 0.13 mJ dose resulted in photoreceptor cell death (*K*). INL, inner nuclear layer; GCL, ganglion cell layer. Quantitative data are presented as mean ± SEM, $n = 3$ analyzed using a 1-way ANOVA. $^{**}P < 0.01$. Scale bar, 50 μm.

Nanosecond laser produces a limited mononuclear cell response

Mononuclear cells such as macrophages and microglia (the resident immune cell of the CNS) are known to remove cellular debris and facilitate healing (57, 58). However, an uncontrolled or persistent immune response involving components such as microglial activation and/or complement cascade involvement can lead to ongoing retinal pathology, and may contribute to the etiology of AMD (59). Thus, for nanosecond laser treatment to provide a clinical benefit, it ideally should not result in an overt immune response.

To detail the mononuclear cell response in the human retina after nanosecond laser treatment, the region encompassing the clinical dose (0.3 mJ) was labeled with the mononuclear marker, ionized calcium-binding adapter molecule 1 (green). Although the nanosecond laser did not alter retinal structure (similar to data in Fig. 2*C*), the cells previously observed near the tips of the outer segments (see Fig. 2*C*) were here identified to be of mononuclear origin (*e.g.*, lymphocytes, monocytes, macrophages; **Fig. 4*A***). In addition to these cells, the endogenous retinal microglia can be observed to stratify within the 2 retinal plexuses (inner plexiform layer [IPL] and OPL), and microglial processes extend through the ONL toward the laser-treated area (Fig. 4*A*). This microglial response seems to reflect that reported for the normal retina, with cell bodies found within the IPL and OPL, and processes extend throughout the retina, surveying the surrounding tissue environment (60).

The microglial response to nanosecond laser treatment was further investigated in the mouse retina. Similar to the human data, mouse retinal microglia were observed to send their processes toward the laser treatment site, and their cell bodies remained in the OPL (Fig. 4*B*, inset shows a 3-dimensional rendered image of 2 laser-treated areas). Association of microglial processes with the

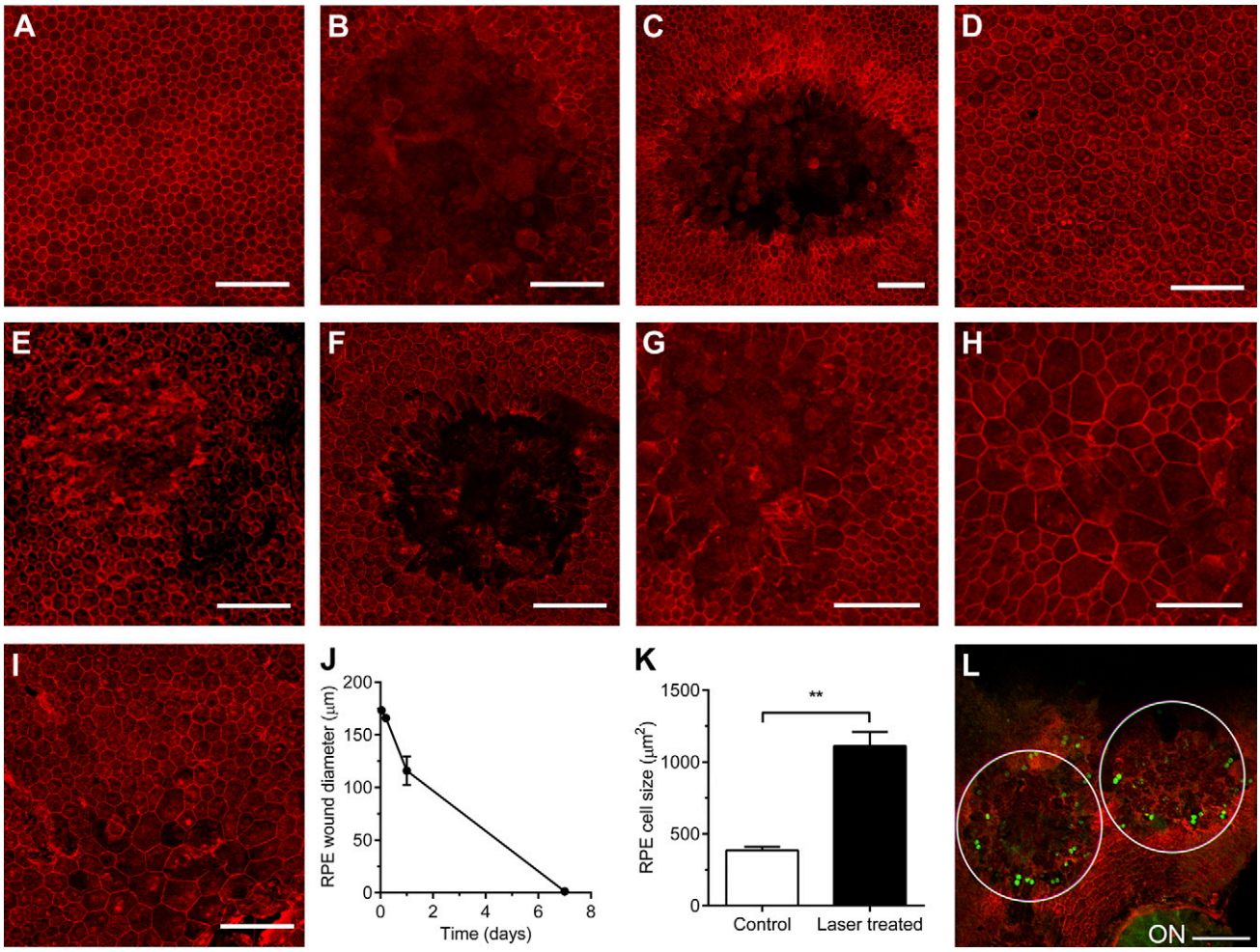

Figure 3. Integrity of human and mouse RPE following nanosecond laser treatment. Five days following nanosecond laser treatment, fixed human retina was flat mounted and the RPE imaged using phalloidin (red), which labels filamentous actin. Normal human RPE morphology (*A*) has a polygonal appearance, and the clinical dose induced a disrupted RPE monolayer (*B*). The RPE lesion was more defined after the suprathreshold laser treatment (0.6 mJ, *C*). Similar to the human, the 0.065 mJ energy treatment of the mouse retina produced a diffuse injury (*E*) compared with the untreated RPE (*D*), and the high dose (0.13 mJ) produced a more defined injury (*F*). One week after nanosecond laser treatment, the treated region in the human showed the presence of larger RPE cells at the injury border, with some cells extending into the lesion site (*G*), and after 1 mo the RPE monolayer was intact (*H*). Seven days post-treatment, the mouse RPE monolayer was reformed with enlarged cells covering the laser-treated site (*I*). This healing process and coincident increase in RPE cell size is quantified (*J, K*, respectively). Twenty-four hours after nanosecond laser (0.065 mJ), mouse RPE cells on the border of the laser treatment site (circles) were positive for cyclin-D1 (red, marker of cell proliferation), while RPE cells distant from the laser spot showed no indication of cyclin-D1 expression (*L*). Quantitative data presented as mean ± SEM; $n > 3$ analyzed using a 2-tailed Student's *t* test. $^{**}P < 0.01$. Scale bar, 100 μm.

photoreceptor outer segments and RPE monolayer can also be observed to be limited to the laser-treated area (Supplemental Fig. 4). Although microglial processes are normally found in the outer retina in the untreated mouse retina, nanosecond laser treatment increased in the number of these processes within the ONL (Fig. 4*C*; 240%, 131 ± 13 *vs.* 54 ± 9; $P < 0.01$). Microglial activation, which is characterized by process retraction and increased soma size (an "amoeboid" phenotype), was characterized in the OPL directly over the laser site. The microglia in the 0.065 mJ treated retinae showed extensive process branching and normal soma sizes (Fig. 4*D*), and microglia directly over the high-energy laser (0.13 mJ) spot showed reduced process branching and a more "amoeboid" appearance (Fig. 4*E*). Quantitative assessment validated these findings, with the clinically equivalent laser dose not resulting in any of the classic signs of microglial activation (Fig. 4*F*, all $P > 0.05$).

Finally, the complement response to nanosecond laser treatment was also investigated because its overexpression can lead to RPE/photoreceptor cell death (61). Complement factor-3 (C3) expression, which is a key component of the complement response, was similar to that found in the untreated retina and was confined to the retinal blood vessels (Fig. 4*G, H*). Conversely, high-dose laser treatment that resulted in extensive retinal cell death (Fig. 2*H, J, K*) and microglial activation (Fig. 4*E*), produced extensive C3 expression around the treated area (Fig. 4*I*). Thus, although low-dose nanosecond laser treatment led to an enhanced microglial surveillance of the outer retinae, it was independent of microglial activation and complement cascade involvement.

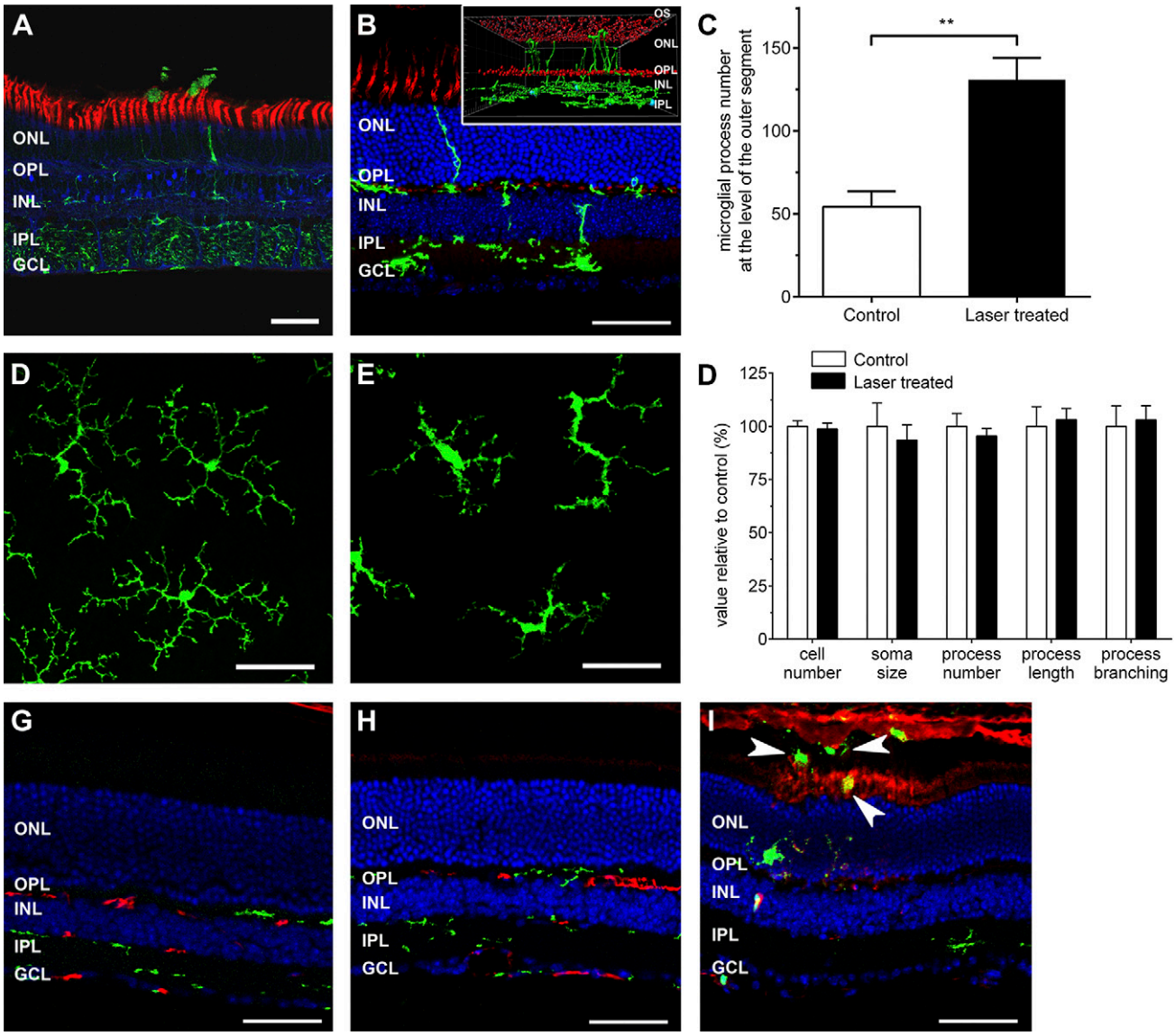

Figure 4. The microglial response in human and mouse retina following nanosecond laser treatment. The human retina was sectioned through the clinically relevant nanosecond laser-treated area and stained with the cone photoreceptor marker, PNA (red); calbindin (blue), which labels numerous cell types in the human retina; and the mononuclear marker, ionized calcium-binding adapter molecule 1 (green). Five days after treatment, cells of mononuclear origin (green) are evident on the distal regions of the outer segments of the photoreceptors (*A*). In addition, retinal microglial cell processes are evident extending toward the laser-treated area. A similar microglial response is observed in the mouse retina 24 h following 0.065 mJ laser treatment (*B,* microglia in green, PNA in red). Three-dimensional reconstruction of the microglial response in the 0.065 mJ-treated mouse retina shows microglial processes extend toward the injury site (inset in *B*, microglia in green, PNA in red). The extension of microglial processes into the outer retina toward the injury site was quantified (*C*). When exposed to low-energy laser dose, retinal microglia were not active (*D*), as a number of their morphologic features common to activation were unchanged (*F*). The high-energy laser treatment (0.13 mJ) resulted in an activated microglial phenotype (*E*). Control (*G*) and low-energy-treated mouse retina (0.065 mJ, *H*) had a similar expression of C3(red; microglia green), with it confined to the retinal blood supply. High-energy laser treatment (0.13 mJ; *I*) resulted in extensive C3 expression and migration of mononuclear cells into the outer retina (see arrows in *I*). All mouse vertical sections were counterstained with the nuclear label, DAPI (blue). OS, outer segment; INL, inner nuclear layer; GCL, ganglion cell layer. Quantitative data presented as mean ± SEM; $n > 4$, analyzed using a 2-tailed Student's *t* test (*C*) and a 2-way ANOVA. $^{**}P < 0.01$. Scale bar, 50 μm.

Nanosecond laser treatment reduces BM thickness

The previous data suggest that the nanosecond laser can reduce drusen load in patients with AMD while sparing the retina from secondary damage and overt inflammation. To investigate whether this treatment may also limit AMD-associated pathology, the ApoEnull mouse was treated with the nanosecond laser (20 laser spots, 0.065 mJ). Although no current model replicates the human disease, this mouse model is known to develop a thickened BM (62), which is one of the hallmark features of AMD.

Retinal/RPE sections were isolated and imaged 3 mo post-treatment. As observed in representative control micrographs (C57BL/6J untreated fellow eye, **Fig. 5*A***), BM

separated the RPE from the choroidal blood supply (Ch) and showed no evidence of rupture or major structural damage after nanosecond laser treatment (Fig. 5*A–D*). Although the control tissue showed a possible minor thinning of BM after laser treatment (Fig. 5*B*), 13 mo ApoEnull animals, which exhibited a thickened membrane (Fig. 5*C*) as previously described (62), appeared dramatically thinner after laser treatment (Fig. 5*D*). When quantified, BM was 47% thicker in ApoE animals compared with age-matched C57BL/6J animals (Fig. 5*E*, 890 ± 60 *vs.* 606 ± 43 nm, $n = 6$, $P < 0.001$). A single nanosecond laser treatment reduced membrane thickness in the ApoEnull by 23% (Fig. 5*E*, 683 ± 38 nm, $P < 0.01$) and resulted in BM thickness not being significantly different from C57BL/6J age-matched animals (683 ± 38 *vs.* 606 ± 43 nm, $P > 0.05$). Importantly, these changes in thickness were observed across the retina and not just in the areas immediately adjacent to sites of nanosecond laser treatment. There was no significant difference between the treated and fellow eyes in the control C57BL/6J animals (Fig. 5*E*; 523 ± 14 *vs.* 606 ± 43 nm, $P > 0.05$), and BM thickness in the fellow eye from the laser-treated ApoEnull animals was not significantly different from either the treated eye (Fig. 5*E*, 795 ± 20 *vs.* 683 ± 38 nm, $P > 0.05$) or the untreated ApoEnull animals (Fig. 5*E*; 795 ± 20 *vs.* 890 ± 60 nm, $P > 0.05$).

ECM turnover is known to be critical for regulation of BM thickness (63, 64). Total RNA was isolated from RPE-choroidal samples and a commercial PCR array was used to screen 84 ECM-related genes from the ApoEnull untreated, ApoEnull laser-treated, and ApoEnull fellow eye samples. When comparing the laser-treated ApoEnull cohort with the untreated ApoEnull, the expression of 21 genes were significantly altered (Supplemental Table 1), encoding ECM proteins such as collagen (*Col1a1, Col5a1, Col4a2*) and laminin (*Lama2, Lamb2, Lamc1*), as well as ECM regulating enzymes (*Mmp3, Mmp2, Timp2*). Of those genes, 9 were regulated greater than 2-fold (Fig. 5*F*), with *Mmp3* up-regulated by the greatest degree (4.5 ± 1.9-fold), and the gene encoding the integrin subunit β4 (*Itgb4*) was decreased (−2.8 ± 0.1-fold). Interestingly, when the fellow eye from the ApoEnull laser-treated animal was compared with the untreated ApoEnull, 72% of the genes altered in the treated eye were also changed to a similar extent in the fellow eye (which did not receive any laser treatment; Supplemental Table 2).

Gene expression of the key matrix degrading enzymes, *Mmp2* and *Mmp3,* were subsequently quantified in all cohorts using quantitative PCR. As observed in Fig. 5*G*, *Mmp2* expression was unchanged in the C57BL/6J laser-treated or fellow eyes when compared with the untreated control samples (treated 0.87 ± 0.09, fellow 0.88 ± 0.09, control 0.89 ± 0.05, $P > 0.05$). By comparison, untreated control ApoEnull RPE-choroidal samples exhibited a 58% reduction in *Mmp2* expression when compared with control C57BL/6J samples (0.37 ± 0.07 *vs.* 0.89 ± 0.05, $P < 0.01$). When ApoEnull animals were treated with the nanosecond laser, *Mmp2* expression increased in both the treated (262%, 0.97 ± 0.16, $P < 0.001$) and fellow (209%, 0.77 ± 0.11, $P < 0.05$) eyes, with expression levels restored to those observed in the C57BL/6J samples (C57BL/6J samples *vs.* ApoEnull-treated and ApoEnull fellow, $P > 0.05$). *Mmp3* gene expression showed a similar response, with ApoEnull untreated levels significantly reduced compared with the C57BL/6J animals (0.52 ± 0.09 *vs.* 0.94 ± 0.07, $P < 0.05$), while levels were restored to that found in the C57BL/6J samples after laser treatment in both the treated (337%, 1.74 ± 0.35, $P < 0.05$) and fellow (328%, 1.69 ± 0.35, $P < 0.05$) eyes. Although ECM gene expression was altered by nanosecond laser treatment, the expression of genes involved in the regulation of RPE function, RPE-specific protein 65kDa (*Rpe65;* photopigment recycling) and Cathepsin D (*Ctsd;* lysosomal function), were not altered (Supplemental Fig. 5).

DISCUSSION

This study investigated the capacity of a low-energy, subthreshold, nanosecond laser to reduce drusen load independent of outer retinal/RPE change in patients with AMD, detailed the cellular damage profile in human and mouse eyes, and assessed the capacity of a nanosecond laser to modulate BM thickening, one of the key pathologic changes observed in AMD. A single session of nanosecond laser treatment (12 spots) reduced drusen load in patients with AMD compared with a natural history cohort, and there was no evidence of detrimental RPE change, indicative of disease progression. Importantly, the human retinal structural studies showed no retinal damage, particularly to the light-sensitive photoreceptors, when clinically appropriate nanosecond laser dosages were applied. The human and mouse retinae exhibited similar cellular responses to the laser, with the discrete laser injury confined to the RPE monolayer, and recruitment of mononuclear cells and retinal microglial processes into the outer retina. Nanosecond laser treatment of the ApoEnull model of AMD resulted in a significant reduction in BM thickness, with an associated increase in the expression of several ECM genes, including *Mmp2* and *Mmp3*, which returned to age-matched control levels.

Nanosecond laser treatment resolves drusen while preserving retinal structure

Data from the clinical study showed that low-energy nanosecond laser reduced drusen area in 40% of treated patients with AMD after 1 yr, which was maintained out to 2 yr post-treatment (35%). Drusen regression was observed in areas adjacent to nanosecond laser-treated sites, in addition to more distant retinal areas, including the untreated fellow eye (1 yr data). This regression was greater than the spontaneous drusen resolution observed in the natural history cohort and in previous publications (14, 65). The capacity of prophylactic laser treatment to reduce drusen load has been described in multiple studies (27, 44, 66, 67), with loss of drusen also occurring in untreated areas of the retina (67–69). The resolution of drusen in the untreated fellow eye was also reported in the large Complications of Age-related macular degeneration Prevention Trial (CAPT) after thermal laser treatment; however, this effect was delayed and not highlighted (44). Interestingly, such fellow eye effects have been described for the use of nanosecond lasers in treating other ocular diseases, such as glaucoma (53).

In addition to a reduction in drusen load, FAF imaging in areas of drusen regression showed no RPE change in the

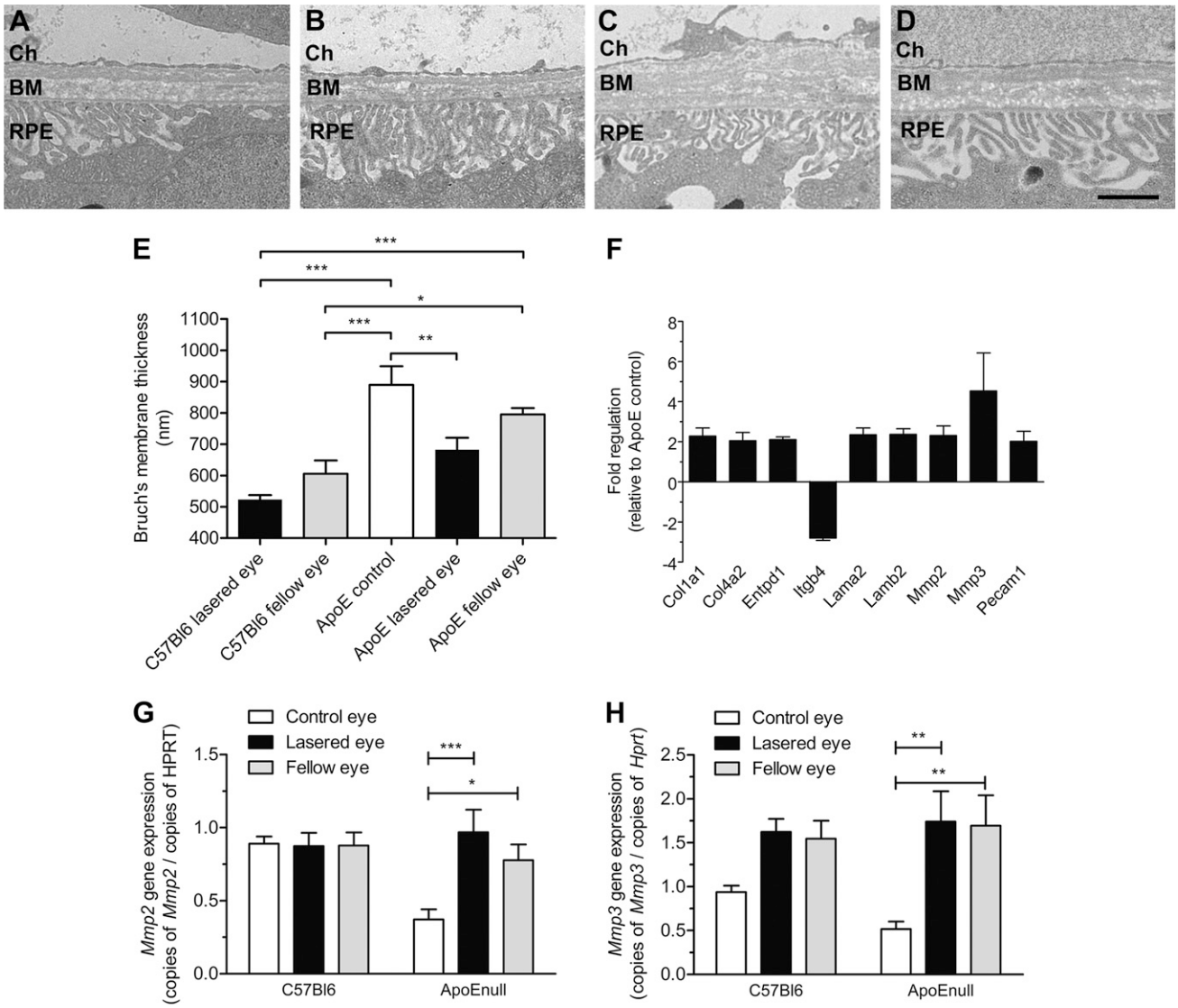

Figure 5. The effect of nanosecond laser treatment on BM thickness and RPE gene expression. ApoEnull and C57BL/6J mice (10 mo of age) were treated with nanosecond laser (20 spots at 0.065 mJ) and tissue taken and fixed after 3 mo. Representative micrographs for C57BL/6J fellow eye (*A*), C57BL/6J treated eye (*B*), ApoEnull fellow eye (*C*), and ApoEnull treated eye (*D*) are shown. BM thickness was quantified (*E*) and showed ApoEnull animals to have a thickened membrane compared with C57BL/6J animals. Nanosecond laser treatment resulted in no significant alteration in BM thickness in the treated eye of C57BL/6J animals; however, there was a mean decrease. By contrast, the laser-treated eye of ApoEnull animals showed a significant reduction in membrane thickness. PCR array data showed 9 ECM genes were regulated >2-fold within the RPE samples from ApoEnull laser-treated eyes compared with samples from untreated ApoEnull control mice (*F*). The expression of genes encoding *Mmp-2* (*G*) and *Mmp-3* (*H*) were quantified and both were reduced in the RPE samples from untreated ApoEnull animals, and laser treatment restored levels to those observed in the C57BL/6J animals. Ch, choroid. Quantitative data presented as mean ± SEM; $n > 6$, except in (*F*) where $n = 3$. Data analyzed using a 2-way ANOVA. $^*P < 0.05$, $^{**}P < 0.01$, $^{***}P < 0.001$. Scale bar, 1 μm.

majority of laser-treated eyes (75%), with evidence of disease progression (as evidence by either increased or decreased FAF) observed in only 25% of treated eyes. This is contrasted against a previous report of spontaneous drusen regression in patients with AMD, which showed 78% exhibiting an autofluorescence change indicative of disease progression (47). Furthermore, the human and mouse data show the repaired RPE monolayer exhibits no evidence of associated pathology, with the expression of key genes involved in RPE function (*Rpe65* and *Cathepsin D*) maintained, and *Mmp-2*, *-3* gene expression is restored to age-matched control levels. Thus, not only does nanosecond laser treatment reduce drusen load over and above that observed in untreated patients with AMD, but RPE changes indicative of AMD progression do not appear to accompany this regression, unlike that observed in spontaneous drusen regression.

Treatment with the nanosecond laser of patients with early AMD also showed promising results with respect to progression to advanced disease. Although the natural history cohort showed almost a doubling of eyes with evidence of advanced pathology (5 eyes at 12 mo, increasing to 9 eyes at 24 mo), laser-treated eyes only showed a modest increase during the same time period (3 eyes at 12 mo,

4 eyes at 24 mo). Furthermore, our recently published work showed that of the 11 treated eyes that were deemed to be at the greatest risk of developing advanced disease, 7 improved to such an extent that they were removed of this high-risk category (41). However, due to the small numbers and short follow-up in this safety pilot clinical trial, no statistical difference in progression to late-stage disease was identified. Despite this, our recent publication showed nanosecond laser treatment improved retinal function as assessed by flicker perimetry (41). As a result of these encouraging results, a multicenter randomized clinical trial is underway (NCT01790802) to determine the effectiveness of nanosecond laser treatment at slowing progression to advanced forms of AMD.

Although traditional thermal laser therapy reduces drusen load, the insult results in retinal damage and possibly an increased risk of choroidal neovascularization (25, 35, 70–72). Even other subthreshold treatments, which were thought to target the RPE and result in no retinal damage, have subsequently been shown to produce both short- and long-term damage, particularly involving the photoreceptor layer (36, 73, 74). Anatomic characterization of the human and mouse retinae after nanosecond laser-treatment produced similar results, showing no evidence of neuronal damage, with the overlying photoreceptor outer segments intact. These data support our *in vivo* results (OCT), which showed occasional RPE alterations but no photoreceptor or inner retinal damage (41), and are further supported by previous work with this laser on the rat retina (38). Although nanosecond laser treatment did result in mononuclear cell accumulation and a modified retinal microglial response, the response was limited, with microglia remaining in a ramified state and no evidence of the activation of the complement cascade. Previous work has shown that activated retinal microglia can produce numerous inflammatory mediators (75), and the continued presence of microglia in the outer retina, together with prolonged inflammation, has been implicated in AMD (59, 76). Thus, unlike thermal lasers, treatment with a nanosecond laser can reduce drusen load, without evidence of overt retinal damage or overt ocular inflammation, when used at clinically appropriate doses.

Nanosecond laser thins BM by regulating ECM remodeling

The ApoEnull mouse, which exhibits a thickened BM (62), was treated with nanosecond laser to determine whether such treatment could reverse this key AMD-associated pathology. Control data showed that aged (13 mo) ApoEnull animals develop a thickened BM, as previously reported (62). Importantly, a single treatment session with a nanosecond laser (20 spots, 0.065 mJ) resulted in a significantly thinner membrane 3 mo after treatment. This thinning was observed across the whole tissue and not just in the vicinity of the laser spots. To our knowledge, this is the first evidence that prophylactic laser treatment reduces BM thickness, a key pathologic change in AMD.

As BM is an acellular structure, it depends upon the adjacent RPE and choroid to produce/regulate its structure. In the untreated ApoEnull animals, which showed a thickened BM, *Mmp-2* (gelatinase) and *Mmp-3* (stromelysin-1) gene expression was significantly reduced in RPE-choroidal samples. As both *Mmp-2* and *Mmp-3* are expressed by the RPE (77), are found within BM (78), and degrade ECM components found in the membrane (79), decreased *Mmp* expression would likely increase membrane thickness and would explain the increased BM thickness we and others have found (62). These data are supported by previous human work describing reduced MMP2 expression with increasing age and in patients with AMD, with both conditions showing a thickened BM (63, 80). When the ApoEnull animals were treated with nanosecond laser, *Mmp-2* and *Mmp-3* expression was restored to those of age-matched controls. The laser-induced increase in *Mmp2* expression confirm previous *in vitro* studies using the nanosecond laser and microsecond pulsed lasers, which show increased basal (toward BM) release of pro- and active *Mmp-2* levels following treatment (31, 81). A previous study also reported increased MMP-9 levels after laser treatment (31); however, this was not found in our PCR array data. Rather *Mmp-3* expression was increased, which is known to be important for activation of other Mmps, such as Mmp-1, -7, and -9. Importantly, unlike the *in vitro* studies that followed Mmp expression out for a maximum of 14 d, this study showed increased *Mmp2* and *Mmp3* expression 3 mo after laser treatment, suggesting a prolonged laser-induced effect.

In addition to the changes in *Mmp* gene expression, the gene array data also showed nanosecond laser treatment increased the expression of several ECM genes such as collagen (*Col1a1*, *5a1*, *4a2*), laminin (*Lama2*, *Lamb2*, *Lamc1*), and components of elastic fibers (Emilin1), in addition to several integrin subunits. Several of these components show an age-dependent reduction in BM directly adjacent to the RPE, leading to disruption of BM-RPE attachment (82, 83). This alteration was particularly found in areas overlying drusen deposits (82). Thus, a laser-induced increase in these ECM proteins, in addition to increased integrin expression, may improve the attachment of the overlying RPE to BM, inhibit the RPE detachment, and slow the atrophic process observed in AMD (4). In support of this, *in vitro* studies in which ECM deposition and integrin expression was increased, showed improved tiling and survival of RPE cells upon aged BM (84, 85). Thus, nanosecond laser treatment appears capable of reversing some of the key age-related alterations in BM and RPE attachment that predisposes individuals to AMD.

Interestingly, our clinical cohort showed a reduction in drusen within the fellow untreated eyes, and the mouse gene expression data also showed evidence of a nanosecond laser-induced fellow eye effect, with RPE-choroidal expression of *Mmp2*, *Mmp3*, and several other ECM genes increased to a similar degree to that observed in the treated eye. Such binocular effects have been reported previously in studies using monocular treatment paradigms, including 1 study involving the nanosecond laser (44, 53). Despite this, the fellow eye effect was not observed with respect to BM, for although there was a mean decrease in thickness in the fellow eye, it was not significant. This apparent disconnect between the matrix gene regulation and membrane thickness may reflect a difference in the temporal nature of the laser-induced effect between the treated and fellow eyes, with longer post-treatment time

required to thin BM in the fellow eye. This is supported by a previous human study that showed drusen resolution after monocular laser treatment to be delayed in the untreated fellow eye (44). It is also possible that a different set of genes were altered in the fellow eyes, compared with the treated eye, resulting in slightly modified response. Nevertheless, given the reduction in drusen within the fellow untreated eyes of our clinical cohort and the nanosecond laser-induced fellow eye effects observed in our mouse model, this binocular effect requires further investigation.

The mechanism for drusen resolution

Drusen regression following prophylactic laser treatment has been reported over many years; however, a mechanism for clearance of drusen remains unclear. Similarly, whether such drusen clearance reflects a slowing of disease progression is unknown. Our human and mouse data support previous *in vitro* studies (22, 23, 31, 86) and suggest an important role for RPE-choroidal cells and BM in facilitating drusen removal. Our data show that nanosecond laser treatment results in a specific alteration in ECM-regulating factors within the RPE-choroidal cells. This laser-induced RPE alteration has previously been hypothesized by Frennesson and Nilsson (32); however, they suggested the newly formed RPE could better phagocytose drusen material. By contrast, our data support a specific matrix-mediated effect rather than a change in RPE metabolism, because the expression of cathepsin-D and RPE65 (markers of RPE lysosomal action and opsin recycling; Supplemental Fig. 5) were not altered by the laser. As BM relies on RPE-choroidal cells to mediate its structure, this altered matrix regulation would likely lead to the thinned membrane observed in the laser-treated ApoEnull animals. In addition to BM thickness, the movement of molecules through the membrane is critical to the influx of important nutrients and the removal of waste products. Previous work has shown an age-related decline in the transport of molecules across BM, the accumulation of lipid deposits, and drusen-based material and the progression toward AMD (22, 86). Although this study provides no direct assessment of the efficacy of nanosecond laser to improve the conductivity of the membrane, previous work has shown a reduction in BM hydraulic conductivity after Mmp exposure in vitro (23). Therefore, the thinned BM observed in this study, in conjunction with an increased Mmp expression and improved RPE-membrane interaction, is likely to reduce outflow resistance and facilitate removal of drusen, as well as improve overall RPE health and function (23). In addition to direct removal of drusen material *via* BM, the thinned membrane may also facilitate additional immune-mediated removal of accumulated drusen, as has previously been described (29).

This study has shown that prophylactic nanosecond laser treatment can bring about the resolution of drusen in those with AMD, while maintaining normal retinal structure. This is critically important for the light-sensitive photoreceptors that are often damaged in thermal ophthalmic laser treatments. As the human and mouse retina show similar responses to nanosecond laser treatment, the thinning of BM and increase in several membrane constituents that improve RPE-membrane attachment may indicate this laser has the potential to improve membrane structure and function in humans. These improvements are crucial to the health of the retina, as reduced transport across BM is integral to the development of AMD. This study demonstrates biologically relevant pathways by which the nanosecond laser improves the pathologic changes known to be implicated in the development of AMD and as such provides a potentially viable intervention for all those at risk of vision loss from its devastating consequences. FJ

This work was supported by the National Health and Medical Research Council of Australia (#1038220 to E.L.F. and M.P.; #1061418 to E.L.F. and A.I.J.; #1061419 to E.L.F. and K.A.V.), practitioner fellowship (#529905 to R.H.G.) and the Victorian Science Agenda (R.H.G., E.L.F., M.P.), Centre for Clinical Research Excellence Award (#529923 to R.H.G.). The Centre for Eye Research Australia receives Operational Infrastructure Support from the Victorian Government. At the time of this work, M.P. was employed by Ellex R&D Pty Ltd. All other authors declare no competing interests.

REFERENCES

1. United Nations, Department of Economic and Social Affairs, Population Division. (2013) World Population Prospects: The 2012 Revision, Highlights and Advance Tables. Working Paper No. ESA/P/WP.228. Retrieved November 6, 2014, from http://esa.un.org/wpp/Documentation/pdf/WPP2012_HIGHLIGHTS.pdf
2. Congdon, N., O'Colmain, B., Klaver, C. C., Klein, R., Muñoz, B., Friedman, D. S., Kempen, J., Taylor, H. R., and Mitchell, P.; Eye Diseases Prevalence Research Group. (2004) Causes and prevalence of visual impairment among adults in the United States. *Arch. Ophthalmol.* **122**, 477–485
3. Mitchell, P., Smith, W., Attebo, K., and Wang, J. J. (1995) Prevalence of age-related maculopathy in Australia. The Blue Mountains Eye Study. *Ophthalmology* **102**, 1450–1460
4. Khandhadia, S., Cherry, J., and Lotery, A. J. (2012) Age-related macular degeneration. *Adv. Exp. Med. Biol.* **724**, 15–36
5. Ambati, J., and Fowler, B. J. (2012) Mechanisms of age-related macular degeneration. *Neuron* **75**, 26–39
6. Brown, D. M., Kaiser, P. K., Michels, M., Soubrane, G., Heier, J. S., Kim, R. Y., Sy, J. P., and Schneider, S.; ANCHOR Study Group. (2006) Ranibizumab versus verteporfin for neovascular age-related macular degeneration. *N. Engl. J. Med.* **355**, 1432–1444
7. Rosenfeld, P. J., Brown, D. M., Heier, J. S., Boyer, D. S., Kaiser, P. K., Chung, C. Y., and Kim, R. Y.; MARINA Study Group. (2006) Ranibizumab for neovascular age-related macular degeneration. *N. Engl. J. Med.* **355**, 1419–1431
8. Gillies, M. C., Walton, R., Simpson, J. M., Arnold, J. J., Guymer, R. H., McAllister, I. L., Hunyor, A. P., Essex, R. W., Morlet, N., and Barthelmes, D.; Fight Retinal Blindness! Project Investigators. (2013) Prospective audit of exudative age-related macular degeneration: 12-month outcomes in treatment-naive eyes. *Invest. Ophthalmol. Vis. Sci.* **54**, 5754–5760
9. Boekhoorn, S. S., Vingerling, J. R., Witteman, J. C., Hofman, A., and de Jong, P. T. (2007) C-reactive protein level and risk of aging macula disorder: The Rotterdam Study. *Arch. Ophthalmol.* **125**, 1396–1401
10. Guymer, R. H., Tao, L. W., Goh, J. K., Liew, D., Ischenko, O., Robman, L. D., Aung, K., Cipriani, T., Cain, M., Richardson, A. J., Baird, P. N., and Langham, R. (2011) Identification of urinary biomarkers for age-related macular degeneration. *Invest. Ophthalmol. Vis. Sci.* **52**, 4639–4644
11. Ferris III, F. L., Wilkinson, C. P., Bird, A., Chakravarthy, U., Chew, E., Csaky, K., and Sadda, S. R.; Beckman Initiative for Macular Research Classification Committee. (2013) Clinical classification of age-related macular degeneration. *Ophthalmology* **120**, 844–851
12. Hageman, G. S., Luthert, P. J., Victor Chong, N. H., Johnson, L. V., Anderson, D. H., and Mullins, R. F. (2001) An integrated hypothesis that considers drusen as biomarkers of immune-mediated processes at the RPE-Bruch's membrane interface in aging and age-related macular degeneration. *Prog. Retin. Eye Res.* **20**, 705–732

13. Gass, J. D. (1972) Drusen and disciform macular detachment and degeneration. *Trans. Am. Ophthalmol. Soc.* **70**, 409–436
14. Gass, J. D. (1973) Drusen and disciform macular detachment and degeneration. *Arch. Ophthalmol.* **90**, 206–217
15. Sarks, S. H. (1980) Council Lecture. Drusen and their relationship to senile macular degeneration. *Aust. J. Ophthalmol.* **8**, 117–130
16. Sarks, S. H. (1982) Drusen patterns predisposing to geographic atrophy of the retinal pigment epithelium. *Aust. J. Ophthalmol.* **10**, 91–97
17. Rudolf, M., Clark, M. E., Chimento, M. F., Li, C. M., Medeiros, N. E., and Curcio, C. A. (2008) Prevalence and morphology of druse types in the macula and periphery of eyes with age-related maculopathy. *Invest. Ophthalmol. Vis. Sci.* **49**, 1200–1209
18. Bressler, S. B., Maguire, M. G., Bressler, N. M., and Fine, S. L.; The Macular Photocoagulation Study Group. (1990) Relationship of drusen and abnormalities of the retinal pigment epithelium to the prognosis of neovascular macular degeneration. *Arch. Ophthalmol.* **108**, 1442–1447
19. Karampelas, M., Sim, D. A., Keane, P. A., Papastefanou, V. P., Sadda, S. R., Tufail, A., and Dowler, J. (2013) Evaluation of retinal pigment epithelium-Bruch's membrane complex thickness in dry age-related macular degeneration using optical coherence tomography. *Br. J. Ophthalmol.* **97**, 1256–1261
20. Starita, C., Hussain, A. A., Pagliarini, S., and Marshall, J. (1996) Hydrodynamics of ageing Bruch's membrane: implications for macular disease. *Exp. Eye Res.* **62**, 565–572
21. Pauleikhoff, D., Chen, J. C., Chisholm, I. H., and Bird, A. C. (1990) Choroidal perfusion abnormality with age-related Bruch's membrane change. *Am. J. Ophthalmol.* **109**, 211–217
22. Hussain, A. A., Starita, C., Hodgetts, A., and Marshall, J. (2010) Macromolecular diffusion characteristics of ageing human Bruch's membrane: implications for age-related macular degeneration (AMD). *Exp. Eye Res.* **90**, 703–710
23. Ahir, A., Guo, L., Hussain, A. A., and Marshall, J. (2002) Expression of metalloproteinases from human retinal pigment epithelial cells and their effects on the hydraulic conductivity of Bruch's membrane. *Invest. Ophthalmol. Vis. Sci.* **43**, 458–465
24. Barathi, V. A., Yeo, S. W., Guymer, R. H., Wong, T. Y., and Luu, C. D. (2014) Effects of simvastatin on retinal structure and function of a high-fat atherogenic mouse model of thickened Bruch's membrane. *Invest. Ophthalmol. Vis. Sci.* **55**, 460–468
25. Olk, R. J., Friberg, T. R., Stickney, K. L., Akduman, L., Wong, K. L., Chen, M. C., Levy, M. H., Garcia, C. A., and Morse, L. S. (1999) Therapeutic benefits of infrared (810-nm) diode laser macular grid photocoagulation in prophylactic treatment of nonexudative age-related macular degeneration: two-year results of a randomized pilot study. *Ophthalmology* **106**, 2082–2090
26. Guymer, R. H., Gross-Jendroska, M., Owens, S. L., Bird, A. C., and Fitzke, F. W. (1997) Laser treatment in subjects with high-risk clinical features of age-related macular degeneration. Posterior pole appearance and retinal function. *Arch. Ophthalmol.* **115**, 595–603
27. Parodi, M. B., Virgili, G., and Evans, J. R. (2009) Laser treatment of drusen to prevent progression to advanced age-related macular degeneration. *Cochrane Database Syst. Rev.* (3):CD006537
28. Guymer, R. H., Hageman, G. S., and Bird, A. C. (2001) Influence of laser photocoagulation on choroidal capillary cytoarchitecture. *Br. J. Ophthalmol.* **85**, 40–46
29. Duvall, J., and Tso, M. O. (1985) Cellular mechanisms of resolution of drusen after laser coagulation. An experimental study. *Arch. Ophthalmol.* **103**, 694–703
30. Yamamoto, C., Ogata, N., Yi, X., Takahashi, K., Miyashiro, M., Yamada, H., Uyama, M., and Matsuzaki, K. (1996) Immunolocalization of basic fibroblast growth factor during wound repair in rat retina after laser photocoagulation. *Graefes Arch. Clin. Exp. Ophthalmol.* **234**, 695–702
31. Zhang, J. J., Sun, Y., Hussain, A. A., and Marshall, J. (2012) Laser-mediated activation of human retinal pigment epithelial cells and concomitant release of matrix metalloproteinases. *Invest. Ophthalmol. Vis. Sci.* **53**, 2928–2937
32. Frennesson, C., and Nilsson, S. E. (1998) Prophylactic laser treatment in early age related maculopathy reduced the incidence of exudative complications. *Br. J. Ophthalmol.* **82**, 1169–1174
33. Little, H. L., Showman, J. M., and Brown, B. W. (1997) A pilot randomized controlled study on the effect of laser photocoagulation of confluent soft macular drusen. *Ophthalmology* **104**, 623–631
34. Friberg, T. R., Musch, D. C., Lim, J. I., Morse, L., Freeman, W., and Sinclair, S. (2006) Prophylactic treatment of age-related macular degeneration report number 1: 810-nanometer laser to eyes with drusen. Unilaterally eligible patients. *Ophthalmology* **113**, 622.e1
35. Choroidal Neovascularization Prevention Trial Research Group. (2003) Laser treatment in fellow eyes with large drusen: updated findings from a pilot randomized clinical trial. *Ophthalmology* **110**, 971–978
36. Mojana, F., Brar, M., Cheng, L., Bartsch, D. U., and Freeman, W. R. (2011) Long-term SD-OCT/SLO imaging of neuroretina and retinal pigment epithelium after subthreshold infrared laser treatment of drusen. *Retina* **31**, 235–242
37. Wood, J. P., Plunkett, M., Previn, V., Chidlow, G., and Casson, R. J. (2011) Nanosecond pulse lasers for retinal applications. *Lasers Surg. Med.* **43**, 499–510
38. Wood, J. P., Shibeeb, O., Plunkett, M., Casson, R. J., and Chidlow, G. (2013) Retinal damage profiles and neuronal effects of laser treatment: comparison of a conventional photocoagulator and a novel 3-nanosecond pulse laser. *Invest. Ophthalmol. Vis. Sci.* **54**, 2305–2318
39. Chidlow, G., Shibeeb, O., Plunkett, M., Casson, R. J., and Wood, J. P. (2013) Glial cell and inflammatory responses to retinal laser treatment: comparison of a conventional photocoagulator and a novel, 3-nanosecond pulse laser. *Invest. Ophthalmol. Vis. Sci.* **54**, 2319–2332
40. Pelosini, L., Hamilton, R., Mohamed, M., Hamilton, A. M., and Marshall, J. (2013) Retina rejuvenation therapy for diabetic macular edema: a pilot study. *Retina* **33**, 548–558
41. Guymer, R. H., Brassington, K. H., Dimitrov, P., Makeyeva, G., Plunkett, M., Xia, W., Chauhan, D., Vingrys, A., and Luu, C. D. (2014) Nanosecond-laser application in intermediate AMD: 12-month results of fundus appearance and macular function. *Clin. Experiment. Ophthalmol.* **42**, 466–479
42. Jung, S., Aliberti, J., Graemmel, P., Sunshine, M. J., Kreutzberg, G. W., Sher, A., and Littman, D. R. (2000) Analysis of fractalkine receptor CX(3)CR1 function by targeted deletion and green fluorescent protein reporter gene insertion. *Mol. Cell. Biol.* **20**, 4106–4114
43. Piedrahita, J. A., Zhang, S. H., Hagaman, J. R., Oliver, P. M., and Maeda, N. (1992) Generation of mice carrying a mutant apolipoprotein E gene inactivated by gene targeting in embryonic stem cells. *Proc. Natl. Acad. Sci. USA* **89**, 4471–4475
44. Complications of Age-Related Macular Degeneration Prevention Trial Research Group. (2006) Laser treatment in patients with bilateral large drusen: the complications of age-related macular degeneration prevention trial. *Ophthalmology* **113**, 1974–1986
45. Delori, F. C., Dorey, C. K., Staurenghi, G., Arend, O., Goger, D. G., and Weiter, J. J. (1995) In vivo fluorescence of the ocular fundus exhibits retinal pigment epithelium lipofuscin characteristics. *Invest. Ophthalmol. Vis. Sci.* **36**, 718–729
46. Schmitz-Valckenberg, S., Fleckenstein, M., Scholl, H. P., and Holz, F. G. (2009) Fundus autofluorescence and progression of age-related macular degeneration. *Surv. Ophthalmol.* **54**, 96–117
47. Toy, B. C., Krishnadev, N., Indaram, M., Cunningham, D., Cukras, C. A., Chew, E. Y., and Wong, W. T. (2013) Drusen regression is associated with local changes in fundus autofluorescence in intermediate age-related macular degeneration. *Am. J. Ophthalmol.* **156**, 532, e1
48. Thévenaz, P., Ruttimann, U. E., and Unser, M. (1998) A pyramid approach to subpixel registration based on intensity. *IEEE Trans. Image Process.* **7**, 27–41
49. Vessey, K. A., Greferath, U., Jobling, A. I., Phipps, J. A., Ho, T., Waugh, M., and Fletcher, E. L. (2012) Ccl2/Cx3cr1 knockout mice have inner retinal dysfunction but are not an accelerated model of AMD. *Invest. Ophthalmol. Vis. Sci.* **53**, 7833–7846
50. Jobling, A. I., Vessey, K. A., Waugh, M., Mills, S. A., and Fletcher, E. L. (2013) A naturally occurring mouse model of achromatopsia: characterization of the mutation in cone transducin and subsequent retinal phenotype. *Invest. Ophthalmol. Vis. Sci.* **54**, 3350–3359
51. Eliasieh, K., Liets, L. C., and Chalupa, L. M. (2007) Cellular reorganization in the human retina during normal aging. *Invest. Ophthalmol. Vis. Sci.* **48**, 2824–2830
52. Vessey, K. A., Wilkinson-Berka, J. L., and Fletcher, E. L. (2011) Characterization of retinal function and glial cell response in a mouse model of oxygen-induced retinopathy. *J. Comp. Neurol.* **519**, 506–527

53. Rhodes, K. M., Weinstein, R., Saltzmann, R. M., Aggarwal, N., Kooner, K. S., Petroll, W. M., and Whitson, J. T. (2009) Intraocular pressure reduction in the untreated fellow eye after selective laser trabeculoplasty. *Curr. Med. Res. Opin.* **25**, 787–796
54. Klein, M. L., Ferris III, F. L., Armstrong, J., Hwang, T. S., Chew, E. Y., Bressler, S. B., and Chandra, S. R.; AREDS Research Group. (2008) Retinal precursors and the development of geographic atrophy in age-related macular degeneration. *Ophthalmology* **115**, 1026–1031
55. Holz, F. G., Bindewald-Wittich, A., Fleckenstein, M., Dreyhaupt, J., Scholl, H. P., and Schmitz-Valckenberg, S.; FAM-Study Group. (2007) Progression of geographic atrophy and impact of fundus autofluorescence patterns in age-related macular degeneration. *Am. J. Ophthalmol.* **143**, 463–472
56. Fletcher, E. L., Jobling, A. I., Vessey, K. A., Luu, C., Guymer, R. H., and Baird, P. N. (2011) Animal models of retinal disease. *Prog. Mol. Biol. Transl. Sci.* **100**, 211–286
57. Eter, N., Engel, D. R., Meyer, L., Helb, H. M., Roth, F., Maurer, J., Holz, F. G., and Kurts, C. (2008) In vivo visualization of dendritic cells, macrophages, and microglial cells responding to laser-induced damage in the fundus of the eye. *Invest. Ophthalmol. Vis. Sci.* **49**, 3649–3658
58. Lech, M., Gröbmayr, R., Weidenbusch, M., and Anders, H. J. (2012) Tissues use resident dendritic cells and macrophages to maintain homeostasis and to regain homeostasis upon tissue injury: the immunoregulatory role of changing tissue environments. *Mediators Inflamm.* **2012**, 951390
59. Ambati, J., Atkinson, J. P., and Gelfand, B. D. (2013) Immunology of age-related macular degeneration. *Nat. Rev. Immunol.* **13**, 438–451
60. Diaz-Araya, C. M., Provis, J. M., Penfold, P. L., and Billson, F. A. (1995) Development of microglial topography in human retina. *J. Comp. Neurol.* **363**, 53–68
61. Cashman, S. M., Desai, A., Ramo, K., and Kumar-Singh, R. (2011) Expression of complement component 3 (C3) from an adenovirus leads to pathology in the murine retina. *Invest. Ophthalmol. Vis. Sci.* **52**, 3436–3445
62. Dithmar, S., Curcio, C. A., Le, N. A., Brown, S., and Grossniklaus, H. E. (2000) Ultrastructural changes in Bruch's membrane of apolipoprotein E-deficient mice. *Invest. Ophthalmol. Vis. Sci.* **41**, 2035–2042
63. Kumar, A., El-Osta, A., Hussain, A. A., and Marshall, J. (2010) Increased sequestration of matrix metalloproteinases in ageing human Bruch's membrane: implications for ECM turnover. *Invest. Ophthalmol. Vis. Sci.* **51**, 2664–2670
64. Kamei, M., and Hollyfield, J. G. (1999) TIMP-3 in Bruch's membrane: changes during aging and in age-related macular degeneration. *Invest. Ophthalmol. Vis. Sci.* **40**, 2367–2375
65. Bressler, N. M., Munoz, B., Maguire, M. G., Vitale, S. E., Schein, O. D., Taylor, H. R., and West, S. K. (1995) Five-year incidence and disappearance of drusen and retinal pigment epithelial abnormalities. Waterman study. *Arch. Ophthalmol.* **113**, 301–308
66. Rodanant, N., Friberg, T. R., Cheng, L., Aurora, A., Bartsch, D., Toyoguchi, M., Corbin, P. S., El-Bradey, M. H., and Freeman, W. R. (2002) Predictors of drusen reduction after subthreshold infrared (810 nm) diode laser macular grid photocoagulation for nonexudative age-related macular degeneration. *Am. J. Ophthalmol.* **134**, 577–585
67. Figueroa, M. S., Regueras, A., and Bertrand, J. (1994) Laser photocoagulation to treat macular soft drusen in age-related macular degeneration. *Retina* **14**, 391–396
68. Gass, J. D. (1971) Photocoagulation of macular lesions. *Trans. Am. Acad. Ophthalmol. Otolaryngol.* **75**, 580–608
69. Sigelman, J. (1991) Foveal drusen resorption one year after perifoveal laser photocoagulation. *Ophthalmology* **98**, 1379–1383
70. Birngruber, R., Gabel, V. P., and Hillenkamp, F. (1983) Experimental studies of laser thermal retinal injury. *Health Phys.* **44**, 519–531
71. Roider, J., Michaud, N., Flotte, T., and Birngruber, R. (1993) [Histology of retinal lesions after continuous irradiation and selective micro-coagulation of the retinal pigment epithelium]. *Ophthalmologe* **90**, 274–278
72. Wallow, I. H., and Tso, M. O. (1973) Repair after xenon arc photocoagulation. 2. A clinical and light microscopic study of the evolution of retinal lesions in the rhesus monkey. *Am. J. Ophthalmol.* **75**, 610–626
73. Pollack, J. S., Kim, J. E., Pulido, J. S., and Burke, J. M. (1998) Tissue effects of subclinical diode laser treatment of the retina. *Arch. Ophthalmol.* **116**, 1633–1639
74. Lanzetta, P., Polito, A., and Veritti, D. (2008) Subthreshold laser. *Ophthalmology* **115**, 216, e1
75. Kaur, C., Rathnasamy, G., and Ling, E. A. (2013) Roles of activated microglia in hypoxia induced neuroinflammation in the developing brain and the retina. *J. Neuroimmune Pharmacol.* **8**, 66–78
76. Chen, J., Connor, K. M., and Smith, L. E. (2007) Overstaying their welcome: defective CX3CR1 microglia eyed in macular degeneration. *J. Clin. Invest.* **117**, 2758–2762
77. Alexander, J. P., Bradley, J. M., Gabourel, J. D., and Acott, T. S. (1990) Expression of matrix metalloproteinases and inhibitor by human retinal pigment epithelium. *Invest. Ophthalmol. Vis. Sci.* **31**, 2520–2528
78. Guo, L., Hussain, A. A., Limb, G. A., and Marshall, J. (1999) Age-dependent variation in metalloproteinase activity of isolated human Bruch's membrane and choroid. *Invest. Ophthalmol. Vis. Sci.* **40**, 2676–2682
79. Booij, J. C., Baas, D. C., Beisekeeva, J., Gorgels, T. G., and Bergen, A. A. (2010) The dynamic nature of Bruch's membrane. *Prog. Retin. Eye Res.* **29**, 1–18
80. Hussain, A. A., Lee, Y., Zhang, J. J., and Marshall, J. (2011) Disturbed matrix metalloproteinase activity of Bruch's membrane in age-related macular degeneration. *Invest. Ophthalmol. Vis. Sci.* **52**, 4459–4466
81. Treumer, F., Klettner, A., Baltz, J., Hussain, A. A., Miura, Y., Brinkmann, R., Roider, J., and Hillenkamp, J. (2012) Vectorial release of matrix metalloproteinases (MMPs) from porcine RPE-choroid explants following selective retina therapy (SRT): towards slowing the macular ageing process. *Exp. Eye Res.* **97**, 63–72
82. Pauleikhoff, D., Wojteki, S., Müller, D., Bornfeld, N., and Heiligenhaus, A. (2000) [Adhesive properties of basal membranes of Bruch's membrane. Immunohistochemical studies of age-dependent changes in adhesive molecules and lipid deposits]. *Ophthalmologe* **97**, 243–250
83. Gullapalli, V. K., Sugino, I. K., Van Patten, Y., Shah, S., and Zarbin, M. A. (2005) Impaired RPE survival on aged submacular human Bruch's membrane. *Exp. Eye Res.* **80**, 235–248
84. Gullapalli, V. K., Sugino, I. K., and Zarbin, M. A. (2008) Culture-induced increase in alpha integrin subunit expression in retinal pigment epithelium is important for improved resurfacing of aged human Bruch's membrane. *Exp. Eye Res.* **86**, 189–200
85. Sugino, I. K., Gullapalli, V. K., Sun, Q., Wang, J., Nunes, C. F., Cheewatrakoolpong, N., Johnson, A. C., Degner, B. C., Hua, J., Liu, T., Chen, W., Li, H., and Zarbin, M. A.. (2011) Cell-deposited matrix improves retinal pigment epithelium survival on aged submacular human Bruch's membrane. *Invest. Ophthalmol. Vis. Sci.* **52**, 1345–1358
86. Moore, D. J., Hussain, A. A., and Marshall, J. (1995) Age-related variation in the hydraulic conductivity of Bruch's membrane. *Invest. Ophthalmol. Vis. Sci.* **36**, 1290–1297

Received for publication August 7, 2014.
Accepted for publication October 2, 2014.